N-Ethylmaleimide–Sensitive Factor b (nsfb) Is Required for Normal Pigmentation of the Zebrafish Retinal Pigment Epithelium

Nicholas J. Hanovice, Christina M. S. Daly, and Jeffrey M. Gross

Eye and Ear Institute, Department of Ophthalmology, Louis J. Fox Center for Vision Restoration, University of Pittsburgh School of Medicine, Pittsburgh, Pennsylvania, United States

Correspondence: Jeffrey M. Gross, Eye and Ear Institute, Department of Ophthalmology, Louis J. Fox Center for Vision Restoration, University of Pittsburgh School of Medicine, Pittsburgh, PA 15213, USA; grossjm@pitt.edu.

Submitted: July 15, 2015
Accepted: October 21, 2015

Citation: Hanovice NJ, Daly CMS, Gross JM. N-ethylmaleimide–sensitive factor b (nsfb) is required for normal pigmentation of the zebrafish retinal pigment epithelium. *Invest Ophthalmol Vis Sci*. 2015;56:7535–7544. DOI:10.1167/iovs.15-17704

Purpose. Despite the number of albinism-causing mutations identified in human patients and animal models, there remain a significant number of cases for which no mutation has been identified, suggesting that our understanding of melanogenesis is incomplete. Previously, we identified two oculocutaneous albinism mutations in zebrafish, *au13* and *au18*. Here, we sought to identify the mutated loci and determine how the affected proteins contribute to normal pigmentation of the retinal pigment epithelium (RPE).

Methods. Complementation analyses revealed that *au13* and *au18* belonged to a single complementation group, suggesting that they affected the same locus. Whole-genome sequencing and single nucleotide polymorphism (SNP) analysis was performed to identify putative mutations, which were confirmed by cDNA sequencing and mRNA rescue. Transmission electron microscopy (TEM) and image quantification were used to identify the cellular basis of hypopigmentation.

Results. Whole-genome sequencing and SNP mapping identified a nonsense mutation in the *N-ethylmaleimide-sensitive factor b* (*nsfb*) gene in *au18* mutants. Complementary DNA sequencing confirmed the presence of the mutation (C893T), which truncates the nsfb protein by roughly two-thirds (Y297X). No coding sequence mutations were identified in *au13*, but quantitative PCR revealed a significant decrease in *nsfb* expression, and *nsfb* mRNA injection rescued the hypopigmentation phenotype, suggesting a regulatory mutation. In situ hybridization revealed that *nsfb* is broadly expressed during embryonic development, including in the RPE. Transmission electron microscopy analyses indicated that average melanosome density and maturity were significantly decreased in *nsfb* mutants.

Conclusions. *au18* and *au13* contain mutations in *nsfb*, which encodes a protein that is required for the maturation of melanosomes in zebrafish RPE.

Keywords: zebrafish, retinal pigment epithelium, oculocutaneous albinism, melanosome

Albinism is a congenital disorder that affects roughly 1 in 17,000 people worldwide[1–3] and is characterized by a complete or partial deficiency of melanin. Ocular defects associated with albinism include nystagmus, foveal hypoplasia, low acuity, and photophobia.[4,5] Hypopigmentation can occur in the eyes and skin (oculocutaneous albinism [OCA]), eyes only (ocular albinism [OA]), or can be accompanied by more severe phenotypes in the relatively rare syndromic forms of albinism, such as Hermansky-Pudlak and Chediak-Higashi syndromes. In all known forms of albinism, hypopigmentation results from mutations in genes encoding proteins involved in melanin synthesis (melanogenesis)[4,6] or in melanosome transport (e.g., Refs. 7, 8).

In the eye, albinism affects the retinal pigment epithelium (RPE), a layer of pigmented cells closely apposed to the photoreceptors at the back of the retina. Proper pigmentation of the RPE is critical for normal retinal development.[9] Melanosomes are specialized lysosome-related organelles that contain pheomelanin and eumelanin pigments. Melanosomes in the RPE aid the visual system by absorbing stray photons to prevent light scatter and focus light onto the photoreceptors.[10] Melanogenesis involves the trafficking of melanogenic enzymes to forming melanosomes, facilitating pigment synthesis and deposition, a process that occurs through several well-defined stages.[11–14] In mammals, stage I premelanosomes, still a part of the endocytic pathway, undergo membrane invaginations to form intralumenal vesicles and begin to develop a proteinaceous fibril meshwork. This meshwork becomes fully formed in stage II melanosomes. Melanin precursors and enzymes are trafficked to stage II melanosomes, and melanin aggregates on the surface of the meshwork, generating a stage III melanosome with characteristic pigmented striations. Melanin aggregation continues until the organelle is completely filled in and becomes a mature stage IV melanosome. This process is well conserved amongst vertebrates, the only notable difference being that, in fish, melanin aggregates on the surfaces of intralumenal vesicles instead of on the striated meshwork.[15]

Melanogenesis depends on proper vesicular targeting and membrane fusion. Indeed, mutations in the genes encoding a number of components of the endocytic pathway result in albinism.[6,16] Despite the number of albinism causing mutations identified in human patients and animal models, there remain a

significant number of cases for which no mutation has yet been identified, suggesting that our understanding of the proteins involved in melanogenesis may be incomplete. Forward genetic screens in animal model systems can be very useful in this regard by utilizing a high-throughout and unbiased screening approach to identify mutations in a process of interest. Highlighting this utility, our laboratory previously reported a forward genetic screen that identified ~20 mutations with defects in eye development.[17] Of this collection, two mutants presented with oculocutaneous albinism, and in this study, we report the cloning and characterization of these mutations and identify them as mutant alleles affecting the *N-ethylmaleimide–sensitive factor* (*nsfb*) gene.

N-ethylmaleimide–sensitive factor (Nsf) is a critical regulator of membrane fusion; NSF was initially identified in yeast as an enzyme required for protein transport between Golgi stacks[18,19] and has since been identified as a AAA superfamily (ATPase associated with various cellular activities) protein that consists of three domains: two ATPase domains (D1 and D2) and an N-terminal domain (NSF-N).[20–22] The NSF protomers form a hexamer, and this constitutes part of the soluble NSF attachment protein (SNAP) complex, which mediates vesicular fusion by disassembling SNARE (SNAP receptor) complexes. SNARE complexes form when SNARE proteins on different membranes interact and provide the requisite energy for membrane fusion by forming four-helix bundles and bringing the membranes into close apposition.[23] As a part of the SNAP complex, NSF couples hydrolysis of ATP with the disassembly of SNARE complexes following membrane fusion, freeing individual SNARE proteins to participate in future vesicular fusion events.[22,24,25] Zebrafish possess two *nsf* genes: *nsfa* and *nsfb*.[26] *nsfa* is required for myelination of axons,[27] the secretion of trophic factors during the maturation of hair cell synapses,[28] and neuropeptide-dependent visually mediated background adaptation.[26] In contrast, very little is known about *nsfb*. Here we demonstrate that *nsfb* mutants display hypopigmentation of the RPE, resulting from a defect in melanogenesis.

Methods

Zebrafish Husbandry

Zebrafish were maintained at 28.5°C on a 14-hour light/10-hour dark cycle. Embryos were obtained from the natural spawning of mutant or wild-type parents in pairwise crosses. According to established protocols,[29] embryos were collected and raised at 28.5°C in the dark until they reached appropriate age for experimentation. All animals were treated in accordance with provisions established by the University of Texas at Austin Institutional Animal Care and Use Committee, and experimentation conformed to the ARVO Statement for the Use of Animals in Ophthalmic and Vision Research. Bright field images of live embryos were captured with a Leica MZT 1600F stereomicroscope (Leica, Wetzlar, Germany).

Single Nucleotide Polymorphism Mapping and Genotyping

Heterozygous *au18* carriers in an AB background were outcrossed with wild-type Tübingen (TU) fish to generate a polymorphic mapping line. Two hundred homozygous mutant embryos from four parental mapping pairs were collected, genomic DNA was isolated (DNeasy Blood & Tissue Kit; Qiagen, Valencia, CA, USA), and 1 μg was utilized in whole-genome sequencing at the University of Texas Genomic Sequencing and Analysis Facility. On an Illumina HiSeq 2000 machine (Illumina, San Diego, CA, USA), 82 million paired-end 100-bp sequences were generated for an average genome coverage of 10.9×. To identify putative mutations, sequencing reads were analyzed via the MegaMapper single nucleotide polymorphism (SNP)-mapping pipeline.[30] Complementary DNA sequencing was performed to confirm the putative *nsfb* mutation. To genotype $nsfb^{c893t}$, we utilized dCAPS Finder 2.0[31] to analyze the genomic sequence of nsfb proximal to the SNP and generate the following primers: forward, 5′-agattttgaacaaatacgtgggaggat-3′ and reverse, 5′-tgactgttgacagaggaacc-3′. These primers amplify a 260-bp product with a *Mbo*I restriction site present in wild-type genomic DNA (gDNA), but not in $nsfb^{c893t}$. Amplicons from gDNA generated from individual embryos were digested with *Mbo*I and run on a 3% agarose gel to distinguish wild-type (260 bp) from $nsfb^{c893t}$ (234 bp) bands.

In Situ Hybridization

In situ hybridizations were performed as described.[32,33] For *nsfb* probe synthesis, a partial cDNA fragment of the coding sequence of *nsfb* was cloned by RT-PCR using the followng primers: 5′-agagaccgccaaatgtcagg-3′ and 5-ctaaaaagccacatgtttatcagggc-3′.

Phylogenetic Analysis

Protein sequences of nsf were obtained from Ensembl release 80 (http://www.ensembl.org, in the public domain),[34] the Saccharomyces genome database (SGD project, http://www.yeastgenome.org, in the public domain),[35] WormBase (http://www.wormbase.org, release WS248, in the public domain),[36] and FlyBase (http://flybase.org, in the public domain).[37] These sequences are yeast nsf (SEC18 and YBR080C), *Drosophila* Nsf1 (FBgn0000346) and Nsf2 (FBgn0266464), *C. elegans* NSF (WBGene00003818), *Xenopus* NSF (ENSXETG00000031364), Zebrafish nsfa (ENSDARG00000007654) and nsfb (ENSDARG00000038991), mouse nsf (ENSMUSG00000034187), chimpanzee nsf (ENSPTRG00000009320), and human NSF (NSG00000073969), with yeast AAA protein ORC1 as an outgroup (YML065W). A phylogenetic tree was generated via Geneious alignment (Geneious version 7.1.5, http://www.geneious.com, in the public domain)[38] and bootstrapped 1000 times for statistical analysis.

Quantitative PCR

Quantitative PCR was performed on wild-type, *au18*, and *au13* embryos at 48 hours post fertilization. Ten embryos were collected per each biological replicate ($n = 3$), mRNA was extracted with Trizol Reagent (Life Technologies, Carlsbad, CA, USA) according to the manufacturer's protocol, and potential genomic DNA contaminants were digested with RNAse-free DNAse I (Roche Diagnostics, Mannheim, Germany) before being reverse transcribed into cDNA with the iScript Reverse Transcriptase Kit (Bio-Rad, Hercules, CA, USA). Real-time quantitative PCR was conducted on five technical replicates per biological replicate using SYBR Green and a Via 7 Real-Time PCR System (Life Technologies).

act2b was used as the reference gene, using primers provided as a generous gift by Johann Eberhart (University of Texas at Austin, Austin, TX, USA): forward, 5′-cgagcaggagatgggaacc-3′ and reverse, 5′-caacggaaacgctcattgc-3′, which produce an amplicon of 128 bp. Primers for *nsfb* were as follows: forward, 5′-ggagctttcttggaggctttca-3′ and reverse, 5′-cgctctgtcctttcacctgtt-3′, which amplify 68 bp.[26] Fold change in *nsfb* transcript expression among *au18*, *au13*, and WT was calculated using the relative gene quantification method.[39]

Histology

Embryos were fixed in fresh 4% glutaraldehyde and 2% paraformaldehyde overnight at room temperature, stained in 2% OsO_4, 2% potassium ferrocyanide, and 2% uranyl acetate, and microwave embedded with a modified reduced viscosity Spurr-Quetol-651 resin using a BDMA accelerator (Electron Microscopy Services, Hatfield, PA, USA) via a 30%, 50%, 75%, 100%, and 100% resin/acetone infiltration series. Samples were sectioned using a Leica Ultracut UC7 ultramicrotome at a thickness of 1 μm, stained with 1% toluidine blue and 1% borax, and imaged on a Leica DM2500 at 400× and 1000× magnification.

Transmission Electron Microscopy

Samples were embedded as above, and cut on a Leica Ultracut UC7 ultramicrotome at a thickness of 70 nm. These sections were imaged on a FEI Tecnai transmission electron microscope (FEI, Hillsboro, OR, USA). Reference images were acquired at 390× magnification to locate the optic nerve and ultrastructure of the RPE. Images ($n = 3$) of the RPE were collected from three regions of the RPE, dorsal, central, and ventral, from $n = 3$ fish at 11,500× magnification. Central RPE was defined as the RPE contained within the region 10° to 30° clockwise from a line connecting the middle of the optic nerve head and the lens core. Dorsal RPE was defined as the region included between 80° and 100° clockwise and ventral RPE between 30° and 40° counterclockwise. Images were rotated to orient the RPE on a horizontal line, and the number, size, and maturity of melanosomes were analyzed using ImageJ software (http://imagej.nih.gov/ij/; provided in the public domain by the National Institutes of Health, Bethesda, MD, USA).

Statistical Analysis

Levene's test found that the homoscedasticity assumption is not satisfied in any dataset. Therefore, to determine whether there was a significant difference between sibling and mutant data during each time point, as well as the change over time of each variable within an individual group, the nonparametric Kruskal-Wallis test was applied, and the Mann-Whitney *U* test was performed for pairwise comparisons. Analyses were completed using GraphPad Prism version 6.0f for Mac (GraphPad Software, San Diego, CA, USA; www.graphpad.com, in the public domain).

Results

au13 and *au18* Mutants Display Oculocutaneous Albinism

au13 and *au18* mutants were isolated from an N-nitroso-N-ethylurea mutagenesis screen for recessive mutations affecting eye development in zebrafish.[17] Both *au13* and *au18* mutations are fully penetrant and strikingly similar in phenotype (Fig. 1); *au13* fails to complement the *au18* mutation (data not shown), suggesting that the mutations affect the same gene. Phenotypically, hypopigmentation is noticeable in mutant embryos by 48 hpf (Figs. 1A, 1C), and the degree of hypopigmentation varies in severity, with mild and severe mutants present in the same clutch of embryos. Both severity classes are globally hypopigmented; in mild mutants, small areas of the RPE are completely devoid of pigment, whereas others appear largely normal. Meanwhile, RPE in severely affected mutants contains numerous large regions lacking pigmentation. By 72 hpf, severely affected mutants begin to display early signs of degeneration, and this includes brain necrosis and a slightly curved body axis.

Given the likely allelic relationship between *au13* and *au18* mutants, and their phenotypic similarity, we focused our efforts on further characterizing the eye phenotype of *au18* mutants at 24, 48, 58, and 72 hpf. *au18* mutant embryos are histologically indistinguishable from wild-type siblings at 24 hpf (Supplementary Fig. S1). At 48 hpf, *au18* retinas are slightly microphthalmic and appear to have fewer melanosomes in their RPE compared with wild-type siblings (Figs. 2A–F). This difference in pigmentation becomes more pronounced over time; by 72 hpf, the mutant RPE contains markedly fewer melanosomes than that of wild-type siblings (Figs. 2M–R). Beyond RPE hypopigmentation and mild microphthalmia, some of the most severely affected mutants possessed lens defects where the posterior of the lens was epithelialized (Figs. 2L, 2R). All other aspects of eye development appeared to be relatively normal in both mutants.

au13 and *au18* Phenotypes Are Caused by Mutations in *nsfb*

To identify the causative mutation in *au18*, we performed next-generation sequencing followed by SNP mapping using the MegaMapper analysis pipeline.[30] Whole-genome sequencing of *au18* mutants generated ∼11× average coverage of the zebrafish genome. MegaMapper analysis identified a 6-Mb window on chromosome 12 as the likely location of the causative mutation. Within this window, a C-to-A transversion mutation at nucleotide 893 (C893T) of the *nsfb* coding sequence was predicted to be the mutation underlying the *au18* phenotype. This mutation is predicted to cause a premature stop codon at amino acid 297, truncating nsfb by 60% (S297X). Complementary DNA sequencing confirmed the presence of this mutation in homozygous *au18* mutant embryos and its absence in wild-type embryos (Fig. 3A). Nsfb contains three major domains: an N-terminal binding domain required for its association with SNAP-complex proteins and two ATPase domains, D1 and D2 (Fig. 3A). The first ATPase domain is required for overall ATPase activity of the protein, whereas the second ATPase mediates hexamerization during complex formation.[22,40,41] The early stop codon in *au18* is predicted to truncate the protein within the first ATPase domain (red dotted line, Fig. 3A), likely resulting in nonfunctional nsfb protein. To confirm that this mutation is causative of the *au18* phenotype, we performed an mRNA rescue experiment by injecting full-length $nsfb^{WT}$ and $nsfb^{au18}$ mRNA into homozygous mutant *au18* embryos. Injection of $nsfb^{WT}$ rescued pigmentation in embryos derived from heterozygous *au18* crosses. (131 of 132), whereas $nsfb^{au18}$ failed to rescue the mutant phenotype (74 of 94; Figs. 3B, 3C). Phenotypic rescue of homozygous $nsfb^{au18}$ mutants was confirmed by genotyping in a subset of injected embryos (data not shown).[42] Based on these data, we conclude that *au18* possesses a nonsense mutation in *nsfb* and hereafter refer to this allele as $nsfb^{au18}$ in accordance with zebrafish nomenclature guidelines.

As mentioned above, *au13* fails to complement the $nsfb^{au18}$ mutation, suggesting that they possess mutations in the same gene. However, we were unable to identify a causative mutation in the coding sequence of *nsfb* in *au13* mutants (data not shown). Injection of $nsfb^{WT}$ mRNA rescued the mutant phenotype in embryos from an *au13* heterozygous incross (145 of 148), whereas injection of $nsfb^{au18}$ failed to rescue the pigmentation phenotype in these clutches (46 of 60). Given the noncomplementation between $nsfb^{au18}$ mutants and *au13* mutants, and these rescue data, the most parsimonious explanation is that *au13* possesses a mutation in a regulatory region of *nsfb* that alters transcript expression. To test this possibility, we performed quantitative PCR analysis of

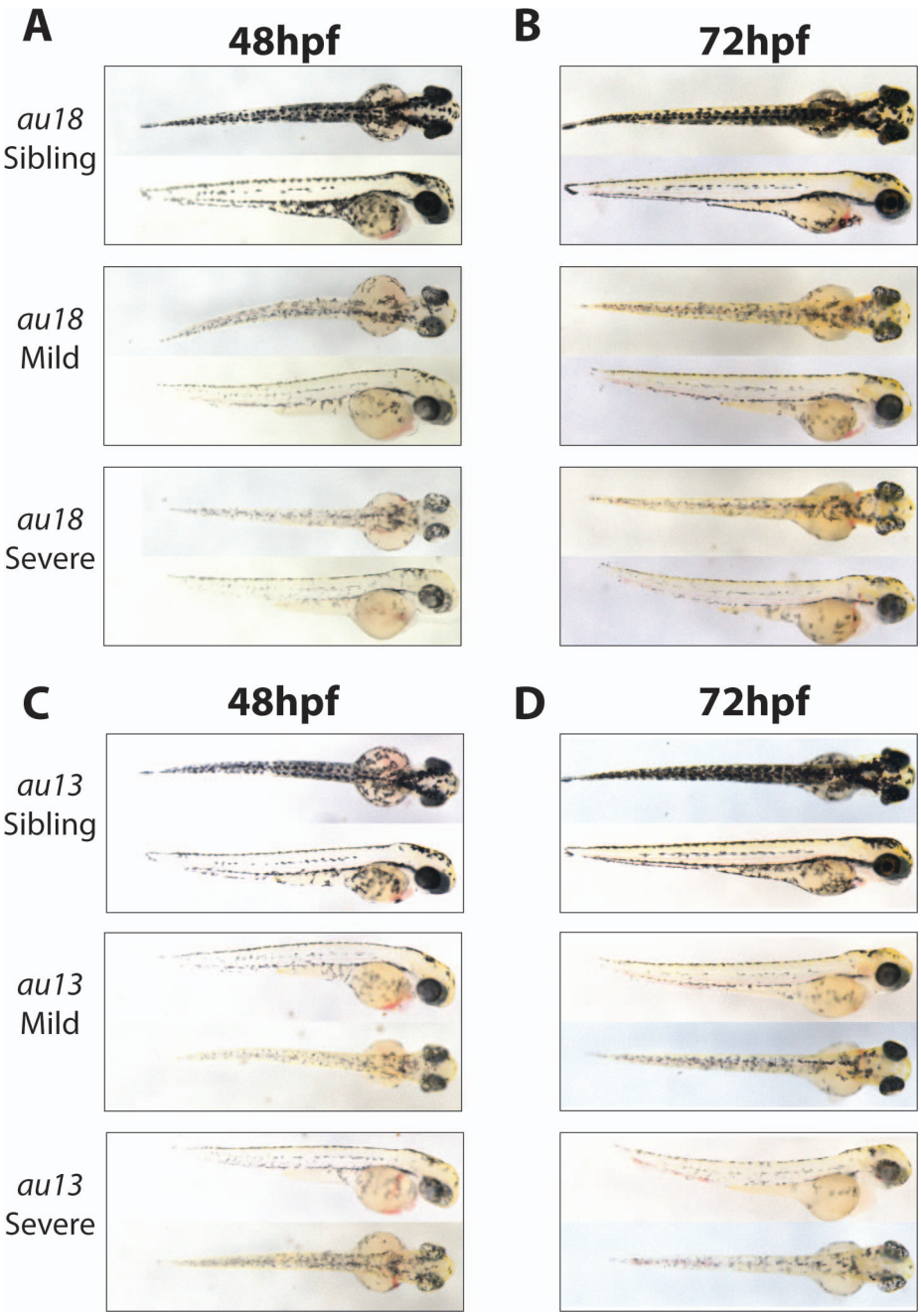

Figure 1. *au18* and *au13* mutants are oculocutaneous albinos. (**A**, **B**) Lateral and dorsal whole embryo images of phenotypically wild-type sibling and mild and severe *au18* mutants at 48hpf and 72hpf. (**C**, **D**) Images of phenotypically wild-type sibling and mild and severe *au13* mutants at 48hpf and 72hpf. In both lines, severe mutants display large regions devoid of pigment in the RPE.

nsfb in *au13* and *nsfb*^{au18} mutants, which revealed that *nsfb* expression was reduced ~2.4-fold in both *nsfb*^{au18} and *au13* relative to wild-type embryos (Fig. 3D). Thus, we conclude that the *au13* phenotype also results from a mutation in *nsfb*, and hereafter refer to this line as *nsfb*^{au13}.

nsfb Is a Ubiquitously Expressed Paralog of Human NSF

The zebrafish genome contains two paralogs of human *NSF*, *nsfa* and *nsfb*, which likely arose from a genome duplication event in teleosts.[43] Phylogenetic analysis of nsf genes suggests that *nsfb* is more distantly related to human *NSF* than *nsfa* (Fig. 4A). The *nsfa* gene is primarily expressed in the nervous system,[27] but the expression pattern of *nsfb* is unknown. In situ hybridization revealed widespread expression, with apparently higher levels of expression in the somites at 24 hpf. At 48 hpf, *nsfb* mRNA expression appears to be more restricted to the anterior half of the embryo, with some enrichment in the otic vesicle and pectoral fins (Fig. 4B).

Melanosome Formation and Maturation Are Disrupted in *nsfb*^{au18} Mutants

Due to the importance of membrane trafficking and vesicular fusion during melanogenesis, we hypothesized that loss of nsfb

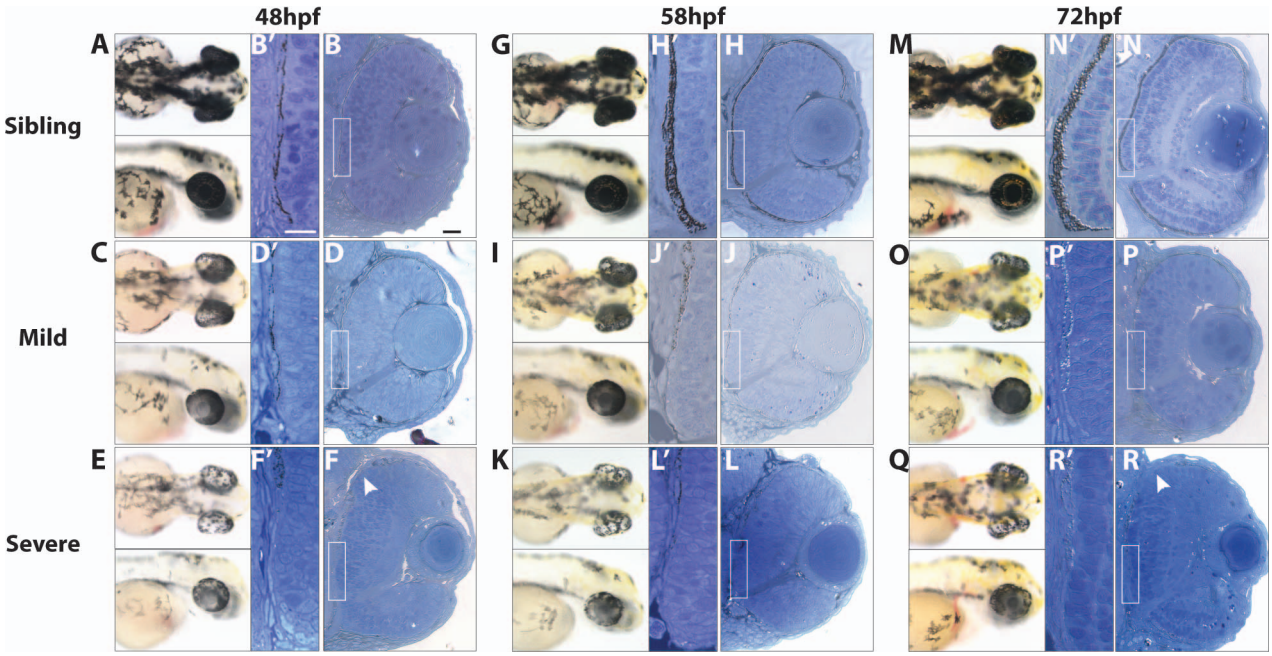

Figure 2. The RPE is disrupted in *au18* mutants. Images of sibling and mutant embryos show that the RPE of *au18* embryos is hypopigmented at 48 (**A**, **C**, **E**), 58 (**G**, **I**, **K**), and 72 hpf (**M**, **O**, **Q**). Transverse histologic sections of sibling and mutant embryos at 48 (**B**, **D**, **F**) 58 (**H**, **J**, **L**), and 78 hpf (**N**, **P**, **R**) reveal that *au18* eye is microphthalmic, but overall retina structure appears to be normal. Areas devoid of pigment are marked by *white arrowheads*. *Scale bar*: 20 μm. (**B′**, **D′**, **F′**, **H′**, **J′**, **L′**, **N′**, **P′**, **R′**) Magnified images of RPE show that RPE proximal to the optic nerve was consistently depigmented in *au18* and confirm that *au18* RPE appears to have fewer melanosomes than wild-type siblings. The posterior lens also appears to be cataractous in severe *au18* mutants (**F**, **L**, **R**). *Scale bar*: 10 μm.

function results in an arrest in melanosome maturation in *nsfb*^{au18} RPE. To test this hypothesis and assess melanogenesis in the *nsfb*^{au18} RPE, we performed transmission electron microscopy (TEM) of *nsfb*^{au18} mutant and sibling RPE at 48, 58, and 72 hpf, quantifying several aspects of melanosome formation from TEM images taken from the dorsal, central, and ventral regions of the RPE (Figs. 5A, 5B). Because hypopigmentation varies in *nsfb*^{au18} mutants, we continued to separate *nsfb*^{au18} embryos into mildly and severely hypopigmented cohorts to determine whether there were quantitative differences in phenotypes between these groups. Quantification of melanosome density revealed that density increased between 58 and 72 hpf in phenotypically wild-type sibling embryos ($P = 0.001$). The average density of *nsfb*^{au18} mutants was significantly lower than sibling at all time points and did not display a significant change over time (Fig. 5C). Moreover, severely hypopigmented *nsfb*^{au18} mutants contained significantly fewer melanosomes than mild *nsfb*^{au18} mutants at 48 and 72 hpf ($P < 0.0001$).

Because melanosomes accumulate more pigment as they mature,[11] the percentage of each melanosome containing pigment was quantified, and this measure was used as a proxy for melanosome maturity. These analyses revealed that *nsfb*^{au18} melanosomes were significantly less mature than phenotypically wild-type siblings at all time points examined (Fig. 5D), and melanosomes in severe *nsfb*^{au18} mutants were less mature than those in mild *nsfb*^{au18} mutants at 58 and 72 hpf. While phenotypically wild-type melanosomes grew more mature over all time points ($P < 0.0001$), overall melanosomal maturity decreased between 48 and 58 hpf in mildly affected ($P = 0.0004$) and severely affected embryos ($P < 0.0001$).

Finally, quantification of the melanosomal perimeter (Fig. 5E) revealed that the average perimeter of melanosomes in phenotypically wild-type siblings did not significantly differ from mild *nsfb*^{au18} mutants. Melanosomal perimeter also increased significantly in sibling and mildly affected mutants between 48 and 58 hpf ($P < 0.0001$). However, the perimeter of melanosomes in severe *nsfb*^{au18} mutants was significantly reduced compared with sibling at 58 and 72 hpf ($P < 0.0001$). Also, unlike in phenotypically wild-type and mildly affected embryos, the melanosomal perimeter decreased significantly between 48 and 58 hpf in severely affected mutants ($P < 0.0001$; Fig. 5E).

Discussion

Albinism results from mutations in a diverse collection of genes that regulate melanogenesis or melanosome trafficking[44]; however, data from human and animal studies suggest that we do not yet know the full complement of genes required for normal pigmentation. For example, although seven genetic subtypes of OCA have thus far been identified, OCA1A and OCA1B (Mendelian Inheritance in Man [MIM] 203100, 606952), OCA2 (MIM 203200), OCA3 (MIM 20390), OCA4 (MIM 606574), OCA5 (615312), OCA6 (MIM 113750), and OCA7 (MIM 615179), the genes underlying OCA5-7 were discovered only very recently,[45,46] highlighting the probability that there are other undiscovered loci responsible for albinism. Here we report two novel zebrafish oculocutaneous albino mutants and establish a role for nsfb in melanogenesis.

Patients with albinism disorders often present with varying degrees of ocular defects, and these include foveal hypoplasia, nystagmus, and improper retinal axon decussation.[4,5] Despite our growing understanding of the genetic etiology of OA, OCA, and the syndromic types of albinism, we know comparatively less about the molecular and cellular underpinnings of these diseases and how pigmentation affects the visual system. Zebrafish are a powerful model organism for gene discovery and mechanistic analysis of protein function during ocular development and disease due to tractable genetics and the ability to perform a diverse array of molecular, biochemical,

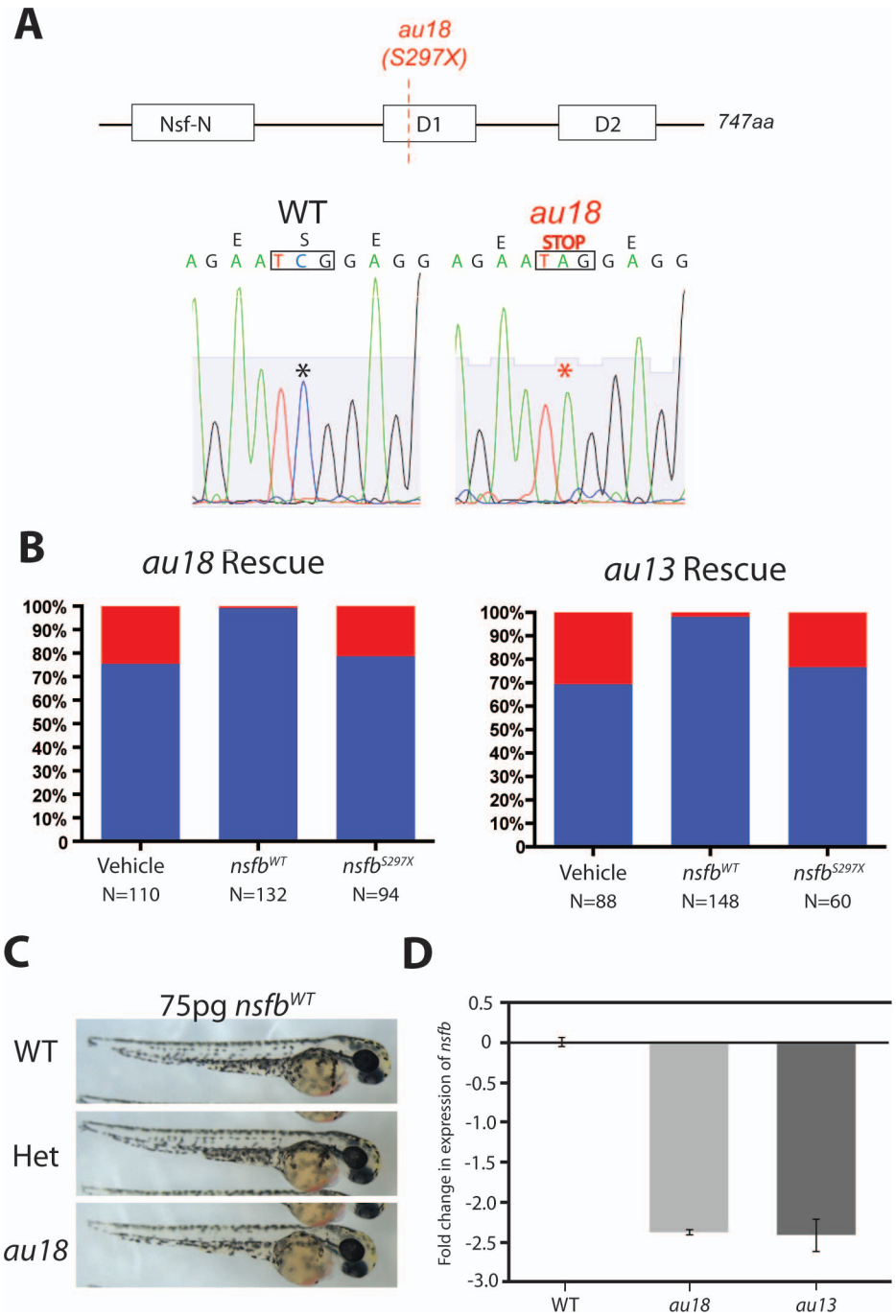

Figure 3. *au13* and *au18* phenotypes are likely caused by mutations in *nsfb*. (**A**) Schematic of the nsfb protein. There are three major domains: the Nsf-N, ATPase domain 1 (D1), and ATPase domain 2 (D2). The mutation occurs at nucleotide 893 (C893T), and the *dotted red line* indicates the location of the premature stop codon at amino acid 297 (S297X) in *au18* mutants. This mutation is predicted to truncate the protein by 60%. (**B**) Graph illustrating the percentage of phenotypically mutant embryos in each clutch following injection of vehicle, $nsfb^{WT}$, and $nsfb^{au18}$ mRNA. Both *au13* and *au18* mutant phenotypes are rescued by injection of $nsfb^{WT}$, whereas injection of $nsfb^{au18}$ mRNA failed to rescue either the *au13* or *au18* mutant phenotype. (**C**) Representative images of WT, $au18^{+/-}$, and $au18^{-/-}$ embryos following $nsfb^{WT}$ injection. (**D**) Quantitative PCR quantification of the relative fold change of *nsfb* in $nsfb^{au13}$ and $nsfb^{au18}$ embryos at 48 hpf. Transcript levels were normalized to *act2b*. *Error bars* indicate SEM of five technical replicates for each experiment. $n = 3$ biological replicates.

anatomic, and behavioral studies.[47,48] Many pigmentation mutants have been identified and characterized in zebrafish,[49–58] some of which directly model existing human pathologies,[59,60] while others presage the identification of human mutations. For example, the causative mutation of OCA6, *SLC24A5*, was identified in a zebrafish pigmentation mutant[61] prior to in the mouse[62] or in human patients.[63] Thus, the zebrafish system represents a potent tool for studying the molecular and cellular regulation of melanogenesis, as well as identifying novel albinism genes in vertebrates.

Here, we report the cloning and characterization of two novel oculocutaneous albino mutants that result from mutations in *nsfb*: $nsfb^{au18}$, which results from a nonsense mutation, and $nsfb^{au13}$, whose causative mutation is unknown

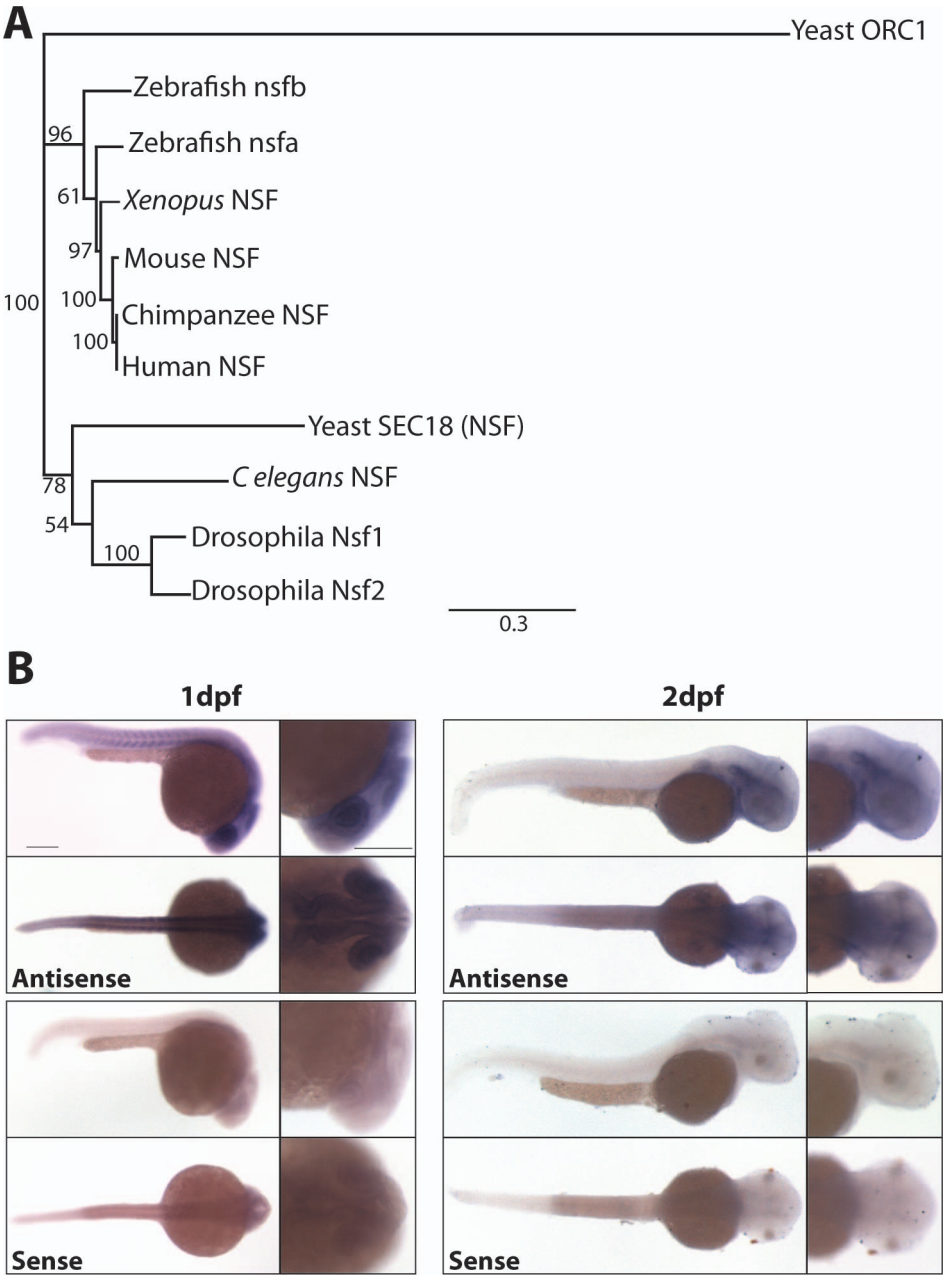

Figure 4. nsfb is a paralog of human NSF and is ubiquitously expressed during early embryo development. (**A**) Phylogenetic analysis of the relationship between nsf in vertebrates. This analysis was constructed using Geneious Tree Builder based on an alignment of nsf amino acid sequences from human, chimpanzee, mouse, *Xenopus*, zebrafish, *Drosophila*, *C. elegans*, and yeast, using yeast Origin recognition complex subunit 1 (ORC1) as an outgroup. Numbers at nodes represent bootstrap values after 1000 replicates. (**B**) In situ hybridization reveals that *nsfb* expression is widespread at 24 hours after fertilization, with higher levels of staining in the somites and nervous system. At 48 hpf, *nsfb* remains widely expressed in the head, with high levels of expression in the otic vesicle and pectoral fins, but is less apparent in the somites and posterior trunk. Lateral and dorsal views of embryos stained for antisense probe are on *top*, and sense controls on *bottom*. *Scale bar*: 200 μm.

but is likely located in a noncoding regulatory region. Indeed, quantitative PCR analysis demonstrated that *nsfb* expression is reduced in *nsfb*^{au13} embryos, supporting this possibility. Interestingly, a comparable reduction of *nsfb* expression was also observed in *nsfb*^{au18} mutant embryos. It is likely that this occurs via nonsense-mediated mRNA decay, a molecular phenotype frequently observed in zebrafish for genes that possess nonsense mutations.[29,61,64,65]

nsfb mutants are oculocutaneous albinos and they are first identifiable at ∼2 dpf based on their hypopigmentation phenotype. *nsfb* is one of the two zebrafish *nsf* paralogs; *Nsf* is ubiquitously expressed in mammals,[66,67] although enriched in the nervous system.[68] *nsfa* expression is limited to the nervous system,[27] whereas *nsfb* has more widespread expression (our data), suggesting that it may be more orthologous in function to *nsf* than *nsfa*. Interestingly, however, our phylogenetic analysis indicates the protein sequence of nsfa is more closely related to human NSF than is nsfb (Fig. 4). Thus, although *nsfb* diverged evolutionarily from mammalian *Nsf*, it possibly retained its system-wide functions, whereas *nsfa* evolved to hold more limited or specialized functions.

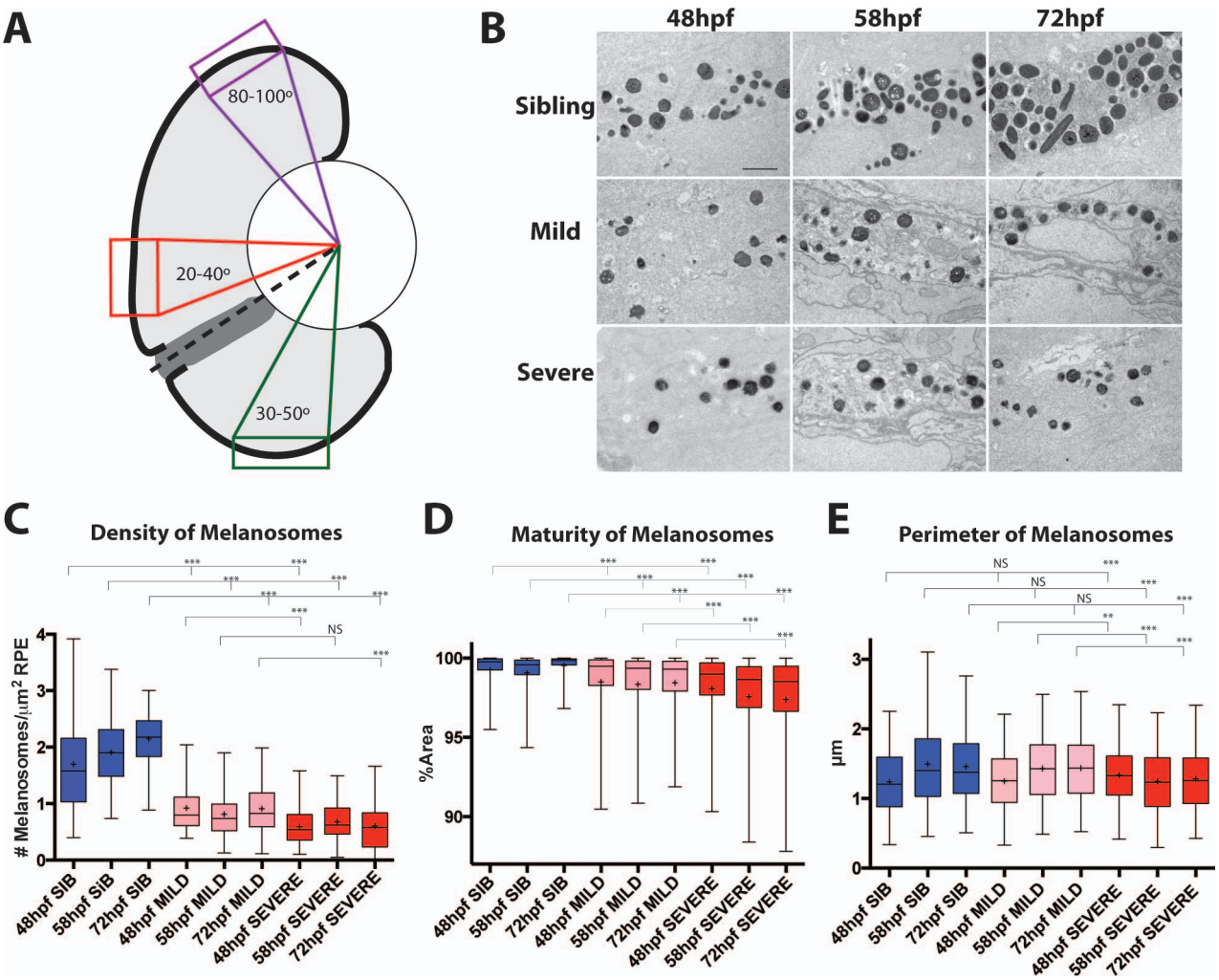

Figure 5. Melanosome formation and maturation is disrupted in *nsfb*^{au18} mutants. (**A**) Cartoon schematic showing the dorsal, central, and ventral regions of the RPE that were analyzed. RPE between 20° and 40° clockwise from an imaginary line (*dotted line*) drawn between the center of the lens and the center of the optic nerve was defined as central, whereas RPE 80° to 100° was defined as dorsal. Finally, RPE contained within a box 30° to 50° counterclockwise was defined as ventral. (**B**) Representative TEM images of central RPE for sibling, mild, and severe *nsfb*^{au18} RPE at 48, 58, and 72 hours after fertilization. Images oriented distal (choroid) up, proximal (retina) down. *Scale bar*: 1 μm. (**C**) Quantification of the average number of melanosomes per square micrometer of RPE indicates that *nsfb*^{au18} mutants contained significantly fewer melanosomes than sibling at all time points, and severe *nsfb*^{au18} mutants contained significantly fewer melanosomes than mild *nsfb*^{au18} mutants at 48 and 72 hpf. (**D**) The graph depicting the average percentage of melanosomes containing pigment reveals that *nsfb*^{au18} melanosomes were significantly less mature than sibling at all time points and that severe mutants were less mature than mild. (**E**) Graph depicting the average perimeter of melanosomes. Although the average perimeter of melanosomes in sibling and mild *nsfb*^{au18} mutants was not significantly different, severe *nsfb*^{au18} melanosomes were significantly smaller than sibling. Furthermore, although melanosomal perimeter increased in sibling and mild RPE, severely affected mutant melanosomes decreased over time. (Mann-Whitney U test, $^{*}P < 0.01$, $^{**}P < 0.001$, $^{***}P < 0.0001$).

Unlike nsfa, virtually nothing is known about the in vivo function(s) of nsfb. Here we demonstrate a critical requirement for nsfb in pigmentation and in regulating the maturation of melanosomes in the RPE. Defects in melanosomal maturation are accompanied by reductions in melanosome number (Fig. 5). Although phenotypes in both *nsfb* alleles were fully penetrant, there were differences in the expressivity of the pigmentation phenotype, with mildly and severely affected mutants detected within the same clutch of homozygous embryos. These data suggest that, although melanogenesis is disrupted in both classes of mutants, it proceeds to a limited extent in mildly affected mutants, whereas it is significantly impaired in severely affected mutants. It is common in zebrafish to have variability of a phenotype,[69–71] and often this variability is ascribed to differing levels of maternal rescue in each embryo resulting from the deposition of mRNAs and proteins into the developing oocyte.[72] More work is necessary to understand the molecular basis of this phenotypic variability in *nsfb* mutants, and, more generally, how maternal rescue contributes to phenotypic variability in recessive zebrafish mutants.

Our quantitative TEM data suggest a model in which nsfb activity is required for the maturation of melanosomes in the RPE. Although we limited our characterization to the RPE hypopigmentation phenotype, *nsfb* mutants possess widespread CNS degeneration by 3 dpf, have reduced circulation, and typically die by 4 dpf. Given the expanded and systemic severity of the phenotypes over those found in ocular albinism or oculocutaneous albinism patients, the *nsfb* phenotypes are more similar to those pathologies observed in patients with syndromic albinism. Indeed, patients with Hermansky Pudlak Syndrome or Chediak-Higashi Syndrome

often have additional, systemic defects such as pulmonary fibrosis and blood clotting defects, in addition to their albinism. Although mutations in *NSF* have not yet been linked to albinism in humans, misregulation of NSF is linked to psychiatric diseases.[73] It will be interesting to screen through existing albinism patients for whom a causative mutation has not yet been identified, particularly those with more syndromic pathologies, to determine whether mutations in NSF underlie their phenotypes. In summary, this study identifies a role for nsfb during melanogenesis in the RPE, establishing an additional and novel oculocutaneous albinism mutant in zebrafish through which the molecular and cellular underpinnings of melanogenesis can be further elucidated.

Acknowledgments

The authors thank Dwight Romanowicz and Trent Reznor for invaluable assistance with TEM, Jacqueline Norrie for assistance with qPCR, Ryoko Minowa for fish care, Etta James for technical assistance, and members of the Gross Laboratory for helpful discussions throughout the course of this work.

Supported by National Institutes of Health Grant R21-EY22700 and CORE Grant P30 EY008098, the Alcon Research Institute, Eye and Ear Foundation of Pittsburgh (Pittsburgh, PA, USA), and an Unrestricted Grant from Research to Prevent Blindness (New York, NY, USA).

Disclosure: **N.J. Hanovice**, None; **C.M.S. Daly**, None; **J.M. Gross**, None

References

1. Hutton SM, Spritz RA. Comprehensive analysis of oculocutaneous albinism among non-Hispanic Caucasians shows that OCA1 is the most prevalent OCA type. *J Invest Dermatol*. 2008;128:2442–2450.
2. Grønskov K, Ek J, Sand A, et al. Birth prevalence and mutation spectrum in Danish patients with autosomal recessive albinism. *Invest Ophthalmol Vis Sci*. 2009;50:1058–1064.
3. Gargiulo A, Testa F, Rossi S, et al. Molecular and clinical characterization of albinism in a large cohort of Italian patients. *Invest Ophthalmol Vis Sci*. 2011;52:1281–1289.
4. Grønskov K, Ek J, Brondum-Nielsen K. Oculocutaneous albinism. *Orphanet J Rare Dis*. 2007;2:43.
5. Levin AV, Stroh E. Albinism for the busy clinician. *J AAPOS*. 2011;15:59–66.
6. Sitaram A, Marks MS. Mechanisms of protein delivery to melanosomes in pigment cells. *Physiology (Bethesda)*. 2012; 27:85–99.
7. Bahadoran P, Aberdam E, Mantoux F, et al. Rab27a: a key to melanosome transport in human melanocytes. *J Cell Biol*. 2001;152:843–849.
8. Griscelli C, Durandy A, Guy-Grand D, Daguillard F, Herzog C, Prunieras M. A syndrome associating partial albinism and immunodeficiency. *Am J Med*. 1978;65:691–702.
9. Jeffery G. The retinal pigment epithelium as a developmental regulator of the neural retina. *Eye (Lond)*. 1998;12(pt 3b): 499–503.
10. Strauss O. The retinal pigment epithelium in visual function. *Physiol Rev*. 2005;85:845–881.
11. Seiji M, Fitzpatrick TB, Simpson RT, Birbeck MS. Chemical composition and terminology of specialized organlles (melanosomes and melanin granules) in mammalian mlanocytes. *Nature*. 1963;197:1082–1084.
12. Seiji M, Shimao K, Birbeck MSC, Fitzpatrick TB. Subcellular localization of melanin biosynthesis. *Ann N Y Acad Sci*. 1963; 100:497–533.
13. Turner WA, Taylor JD, Tchen TT. Melanosome formation in the goldfish: the role of multivesicular bodies. *J Ultrastruct Res*. 1975;31:16–31.
14. Abramowitz J, Turner WA, Chavin W, Taylor JD. Trysinase positive oculocutaneous albinism in the goldfish, *Carassius auratus* l., and ultrastructural and biochemical study of the eye. *Cell Tissue Res*. 1977;182:409–419.
15. Navarro RE, Ramos-Balderas JL, Guerrero I, Pelcastre V, Maldonado E. Pigment dilution mutants from fish models with connection to lysosome-related organelles and vesicular traffic genes. *Zebrafish*. 2008;5:309–318.
16. Huizing M, Helip-wooley A, Westbroek W, Gunay-aygun M, Gahl WA. Disorders of lysosome-related organelle biogenesis: clinical and molecular genetics. *Annu Rev Genomics Hum Genet*. 2008;9:359–386.
17. Lee J, Cox BD, Daly CM, et al. An ENU mutagenesis screen in zebrafish for visual system mutants identifies a novel splice-acceptor site mutation in patched2 that results in Colobomas. *Invest Ophthalmol Vis Sci*. 2012;53:8214–8221.
18. Melançon P, Glick B, Malhotra V. Involvement of GTP-binding 'G' proteins in transport through the Golgi stack. *Cell*. 1987; 51:1053–1062.
19. Block MR, Glick BS, Wilcox CA, Wieland FT, Rothman JE. Purification of an N-ethylmaleimide-sensitive protein catalyzing vesicular transport. *Proc Natl Acad Sci U S A*. 1988;85: 7852–7856.
20. Tagaya M, Wilson DW, Brunner M, Arango N, Rothman JE. Domain structure of an N-ethylmaleimide-sensitive fusion protein involved in vesicular transport. *J Biol Chem*. 1993; 268:2662–2666.
21. Nagiec EE, Bernstein A, Whiteheart SW. Each domain of the N-ethylmaleimide-sensitive fusion protein contributes to its transport activity. *J Biol Chem*. 1995;270:29182–29188.
22. Whiteheart SW, Rossnagel K, Buhrow SA, Brunner M, Jaenicke R, Rothman JE. N-ethylmaleimide-sensitive fusion protein: a trimeric ATPase whose hydrolysis of ATP is required for membrane fusion. *J Cell Biol*. 1994;126:945–954.
23. Jahn R, Scheller RH. SNAREs—engines for membrane fusion. *Nat Rev Mol Cell Biol*. 2006;7:631–643.
24. Banerjee A, Barry VA, DasGupta BR, Martin TFJ. N-ethylmaleimide-sensitive factor acts at a prefusion ATP-dependent step in Ca2+-activated exocytosis. *J Biol Chem*. 1996;271: 20223–20226.
25. May AP, Whiteheart SW, Weis WI. Unraveling the mechanism of the vesicle transport ATPase NSF, the N-ethylmaleimide-sensitive factor. *J Biol Chem*. 2001;276:21991–21994.
26. Kurrasch DM, Nevin LM, Wong JS, Baier H, Ingraham HA. Neuroendocrine transcriptional programs adapt dynamically to the supply and demand for neuropeptides as revealed in NSF mutant zebrafish. *Neural Dev*. 2009;4:221–16.
27. Woods IG, Lyons DA, Voas MG, Pogoda H-M, Talbot WS. Nsf is essential for organization of myelinated axons in zebrafish. *Curr Biol*. 2006;16:636–648.
28. Mo W, Nicolson T. Both pre- and postsynaptic activity of Nsf prevents degeneration of hair-cell synapses. *PLoS One*. 2011;6: e27146.
29. Westerfield M. *The Zebrafish Book: A Guide for the Laboratory Use of Zebrafish (Danio rerio)*. 4th ed. Eugene: University of Oregon Press; 2000.
30. Obholzer N, Swinburne IA, Schwab E, Nechiporuk AV, Nicolson T, Megason SG. Rapid positional cloning of zebrafish mutations by linkage and homozygosity mapping using whole-genome sequencing. *Development*. 2012;139:4280–4290.
31. Lu HH, Neff MM, Turk E, Kalishman M. Web-based primer design for single nucleotide polymorphism analysis. *Trends Genet*. 2002;18:613–615.

32. Jowett T, Lettice L. Whole-mount in situ hybridization zebrafish embryos using a mixture of digoxigenin- and fluorescein-labelled probes. *Trends Genet*. 1994;10:73–74.
33. Thisse C, Thisse B. High-resolution in situ hybridization to whole-mount zebrafish embryos. *Nat Protoc*. 200;3:59–69.
34. Flicek P, Amode MR, Barrell D, et al. Ensembl 2014. *Nucleic Acids Res*. 2014;42:749–755.
35. Engel SR, Dietrich FS, Fisk DG, et al. The reference genome sequence of *Saccharomyces cerevisiae*: then and now. *G3 (Bethesda)*. 2014;4:389–398.
36. Yook K, Harris TW, Bieri T, et al. WormBase 2012: more genomes, more data, new website. *Nucleic Acids Res*. 2012; 40:735–741.
37. Marygold SJ, Leyland PC, Seal RL, et al. FlyBase: improvements to the bibliography. *Nucleic Acids Res*. 2013;41:751–757.
38. Kearse M, Moir R, Wilson A, et al. Geneious Basic: an integrated and extendable desktop software platform for the organization and analysis of sequence data. *Bioinformatics*. 2012;28:1647–1649.
39. Livak KJ, Schmittgen TD. Analysis of relative gene expression data using real-time quantitative PCR and the 2(-Delta Delta C(T)) method. *Methods San Diego Calif*. 2001;25:402–408.
40. Sumida M, Hong R, Tagayas M. Role of two nucleotide-binding regions in an N-ethylmaleimide-sensitive factor involved in vesicle-mediated protein transport. *J Biol Chem*. 1994;269: 20636–20641.
41. Yu RC, Jahn R, Brunger ATNSF. N-terminal domain crystal structure: models of NSF function. *Mol Cell*. 1999;4:97–107.
42. Neff MM, Neff JD, Chory J, Pepper AE. dCAPS, a simple technique for the genetic analysis of single nucleotide polymorphisms: experimental applications in *Arabidopsis thaliana* genetics. *Plant J*. 1998;14:387–392.
43. Amores A, Force A, Yan YL, et al. Zebrafish hox clusters and vertebrate genome evolution. *Science*. 1998;282:1711–1714.
44. Oetting WS, King RA. Molecular basis of albinism: mutations and polymorphisms of pigmentation genes associated with albinism. *Hum Mutat*. 1999;13:99–115.
45. Kausar T, Bhatti M, Ali M, Shaikh R, Ahmed Z. OCA5, a novel locus for non-syndromic oculocutaneous albinism, maps to chromosome 4q24. *Clin Genet*. 2013;84:91–93.
46. Montoliu L, Grønskov K, Wei AH, et al. Increasing the complexity: new genes and new types of albinism. *Pigment Cell Melanoma Res*. 2014;27:11–18.
47. Lieschke GJ, Currie PD. Animal models of human disease: zebrafish swim into view. *Nat Rev Genet*. 2007;8:353–367.
48. Gross J, Perkins B. Zebrafish mutants as models for congenital ocular disorders in humans. *Mol Reprod Dev*. 2008;555:547–555.
49. Streisinger G, Walker C, Dower N, Knauber D, Singer F. Production of clones of homozygous diploid zebra fish (*Brachydanio rerio*). *Nature*. 1981;291:293–296.
50. Kelsh RN, Brand M, Jiang YJ, et al. Zebrafish pigmentation mutations and the processes of neural crest development. *Development*. 1996;123:369–389.
51. Haffter P, Granato M, Brand M, et al. The identification of genes with unique and essential functions in the development of the zebrafish, *Danio rerio*. *Development*. 1996;123:1–36.
52. Odenthal J, Rossnagel K, Haffter P, et al. Mutations affecting xanthophore pigmentation in the zebrafish, *Danio rerio*. *Development*. 1996;123:391–398.
53. Neuhauss SC, Biehlmaier O, Seeliger MW, et al. Genetic disorders of vision revealed by a behavioral screen of 400 essential loci in zebrafish. *J Neurosci*. 1999;19:8603–8615.
54. Golling G, Amsterdam A, Sun Z, et al. Insertional mutagenesis in zebrafish rapidly identifies genes essential for early vertebrate development. *Nat Genet*. 2002;31:135–140.
55. Amsterdam A, Nissen RM, Sun Z, Swindell EC, Farrington S, Hopkins N. Identification of 315 genes essential for early zebrafish development. *Proc Natl Acad Sci U S A*. 2004;101: 12792–12797.
56. Nuckels RJ, Ng A, Darland T, Gross JM. The vacuolar-ATPase complex regulates retinoblast proliferation and survival, photoreceptor morphogenesis, and pigmentation in the zebrafish eye. *Invest Ophthalmol Vis Sci*. 2009;50:893–905.
57. Ng A, Uribe RA, Yieh L, Nuckels R, Gross JM. Zebrafish mutations in gart and paics identify crucial roles for de novo purine synthesis in vertebrate pigmentation and ocular development. *Development*. 2009;136:2601–2611.
58. Daly CMS, Willer J, Gregg R, Gross JM. Snow white, a zebrafish model of Hermansky-Pudlak syndrome type 5. *Genetics*. 2013; 195:481–494.
59. Page-McCaw PS, Chung SC, Muto A, et al. Retinal network adaptation to bright light requires tyrosinase. *Nat Neurosci*. 2004;7:1329–1336.
60. Krauss J, Geiger-Rudolph S, Koch I, Nüsslein-Volhard C, Irion U. A dominant mutation in tyrp1A leads to melanophore death in zebrafish. *Pigment Cell Melanoma Res*. 2014;27: 827–830.
61. Lamason RL, Mohideen MA, Mest JR, et al. SLC24A5, a putative cation exchanger, affects pigmentation in zebrafish and humans. *Science*. 2005;310:1782–1786.
62. Vogel P, Read RW, Vance RB, Platt KA, Troughton K, Rice DS. Ocular albinism and hypopigmentation defects in Slc24a5-/- mice. *Vet Pathol*. 2008;45:264–279.
63. Wei A-H, Zang DJ, Zhang Z, et al. Exome sequencing identifies SLC24A5 as a candidate gene for nonsyndromic oculocutaneous albinism. *J Invest Dermatol*. 2013;133:1834–1840.
64. Fricke C, Lee JS, Geiger-Rudolph S, Bonhoeffer F, Chien CB. Astray, a zebrafish roundabout homolog required for retinal axon guidance. *Science*. 2001;292:507–510.
65. Xiao T, Baier H. Lamina-specific axonal projections in the zebrafish tectum require the type IV collagen Dragnet. *Nat Neurosci*. 2007;10:1529–1537.
66. Visel A, Thaller C, Eichele G. GenePaint.org: an atlas of gene expression patterns in the mouse embryo. *Nucleic Acids Res*. 2004;32:D552–D556.
67. Magdaleno S, Jensen P, Brumwell CL, et al. BGEM: an in situ hybridization database of gene expression in the embryonic and adult mouse nervous system. *PLoS Biol*. 2006;4:497–500.
68. Betz H. The N-ethylmaleimide-sensitive fusion protein (NSF) is preferentially expressed in the nervous system. *FEBS Lett*. 1994;347:55–58.
69. Hartsock A, Lee C, Arnold V, Gross JM. In vivo analysis of hyaloid vasculature morphogenesis in zebrafish: a role for the lens in maturation and maintenance of the hyaloid. *Dev Biol*. 2014;2:1–13.
70. Lee, J, Gross, JM. Laminin B1 and y1 containing laminins are essential for basement membrane integrity in the zebrafish eye. *Invest Ophthalmol Vis Sci*. 2007;48:2483–2490.
71. Lee J, Willer JR, Willer GB, Smith K, Gregg RG, Gross JM. Zebrafish blowout provides genetic evidence for Patched1 mediated negative regulation of Hedghog signaling within the proximal optic vesicle of the vertebrate eye. *Dev Biol*. 2008; 319:10–22.
72. Abrams EW, Mullins MC. Early zebrafish development: it's in the maternal genes. *Curr Opin Genet Dev*. 2010;19:396–403.
73. Imai C, Sugai T, Iritani S, et al. A quantitative study on the expression of synapsin II and N-ethylmaleimide-sensitive fusion protein in schizophrenic patients. *Neurosci Lett*. 2001;305:185–188.